Opt. Soc. Am./Fourier Transform Spectroscopy, Lake Arrowhead, CA, March 1-4, 2015
LLNL-ABS-662476

Phase Stepping Algorithm For Unknown Irregular Steps: Applications in Dispersed Interferometry

David J. Erskine
Lawrence Livermore Nat. Lab., 7000 East Ave, Livermore, CA 94550
erskine1@llnl.gov

Jerry Edelstein
Space Sciences Laboratory, University of California, Berkeley, CA 94720

Abstract: We process externally dispersed interferometer spectral data with a novel phase-stepping algorithm tolerating steps of unknown irregular phase and visibility, which change significantly across a 0.9 to 2.5 μm bandwidth.

OCIS codes: (300.632) Spectroscopy, High Resolution, (120.2650) Fringe analysis, (120.5070) Phase-stepped Interferometry

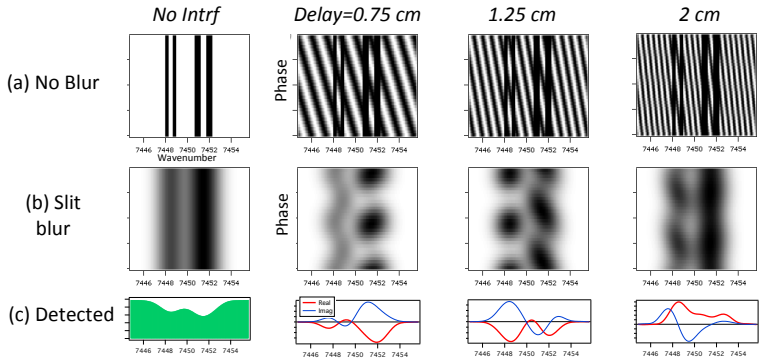

Fig. 1. An EDI superimposes a sinusoidal interferometer comb on an input spectrum, (a) prior to spectrograph slit blurring (b), creating moire patterns which contain originally high spatial frequency information heterodyned to low frequencies. Different interferometer delays cover different frequency ranges. The moire patterns are expressed as a complex spectra (c) using the phase stepping algorithm we developed.

1. Introduction

A novel technique called externally dispersed interferometry [1] (EDI) can dramatically reduce the necessary size of spectrographs for Doppler radial velocimetry [2, 3] and high resolution spectroscopy [4–6]. We have demonstrated EDI in both applications, in the near-infrared at the Hale 5-m telescope at Mt. Palomar Observatory. In EDI an interferometer in series with a dispersive spectrograph creates moire fringes (Fig. 1) between the sinusoidal transmission and the input spectrum. These are high frequency features heterodyned to resolvable lower frequencies. Moire patterns at several interferometer delays τ are later numerically shifted up in Fourier space to restore the original frequencies. This produces a net spectrum having much higher resolution than the native spectrograph by 4x to 10x.

This summary focuses on the novel phase-stepping algorithm we use to separate fringing and nonfringing spectra from the fringing spectral data, that can handle unknown and irregular and steps, and therefore is useful to other interferometry applications. Our EDI data set is a sequence of 10 spectra taken at approximately uniform (0.25 μm) *delay* steps. These have a nonuniform distribution of *phase* steps because the phase ϕ varies with wavelength λ and wavenumber ν across a wide bandwidth (0.9 to 2.5 μm) as $\Delta\phi = \Delta\tau/\lambda = \nu\Delta\tau$. Since ν changes by 1.3 times across a spectrograph order and a factor 2.5 across the four echelle orders (4100 to 10500 cm^{-1}), the phase step is different for each wavenumber. So even if it is regular (evenly distributed across 1 cycle of phase, i.e. 1/10 cycle steps) for

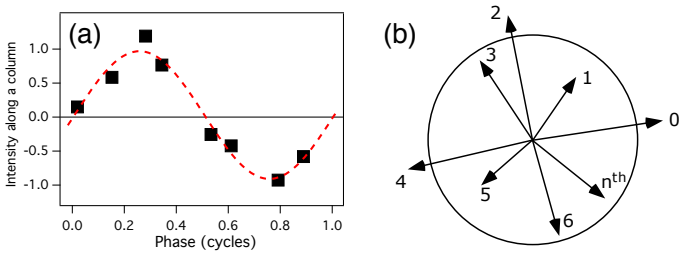

Fig. 2. The sine fitting (a) is similar to a vector construction (b) where step phase and visibility are designated by vector length and angle, which can both be irregular. (Hypothetical points shown.) The vector method handles variable visibility data better, because it does not require magnifying (normalizing) low visibility data, and hence magnifying noise, to achieve uniform visibility prior to the fit. To isolate the nonfringing from fringing components the vector sum must be zero, achieved by adjusting weights.

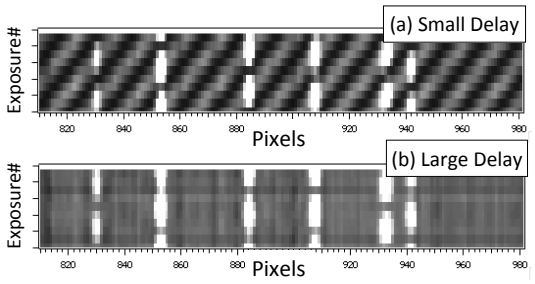

Fig. 3. Example stellar and ThAr spectral lamp fringing data for 10 phase steps (10 rows stacked in an array) vs wavenumber along horizontal axis. Horizontal scaling is $\sim$1 cm^{-1} per pixel, at around 7500 cm^{-1}. (a) Small delay shows resolvable interferometer comb, whereas large delay (b) is unresolvable for the continuum but still shows fringes for the narrow ThAr lines. The phase pattern of ThAr lines is a "fingerprint" that allows determination of step delay change. Unnormallized intensity fluctuations due to atmospheric seeing cause horizontal artifacts in (b).

some wavenumbers, at other wavenumbers it wraps incompletely around the phase circle and produces an unbalanced distribution. Secondly, slight mechanical vibrations, air convection and atmospheric seeing can alter individual step delay and fringe visibility, so we assume for most generality that the phases and visibilities are unknown and irregular. This distinguishes our algorithm from most algorithms in the literature [7], which cannot handle unknown irregular steps.

1.1. On Sine Fitting

For each wavenumber channel (vertical column of Fig. 1), the intensity vs phase is essentially fitted to a sinusoid, where the sine and cosine amplitudes represent the imaginary and real parts of the complex spectrum which represents the moire pattern. In the case of uniform visibility fringes, and knowledge of phase step positions, a sine fitting routine can be used. But if the visibility is nonuniform (as in Fig. 2[a]), such as under atmospheric seeing induced intensity variations or averaged phase wanderings, then a standard sine fitting routine can give an erroneous result. (Magnifying a weak signal also magnifies the photon noise, so fixing severe drops in fringe visibility only through normalization is not recommended.)

We use a vector combination method instead (Fig. 2[b]), which has greater flexibility in handling irregular fringe visibility and irregular phases, and has the ability for massively parallel calculations. To separate the fringing and nonfringing component the vector sum must be zero, and weightings are applied to achieve this. Whatever arithmetic is performed on vectors is also performed on input spectra (intensity) data, for each step. If some of the vectors have near zero magnitude, they simply do not contribute significantly to this sum. It is better to adjust the weightings of the larger (cleaner) vectors to achieve zero. So dropouts in signal due to a passing cloud, for example, are tolerated well in our scheme. Figure 3 shows example raw fringing data array, which is a stack of 10 phase stepped spectra (vertically) along pixel (dispersion direction in horizontal).

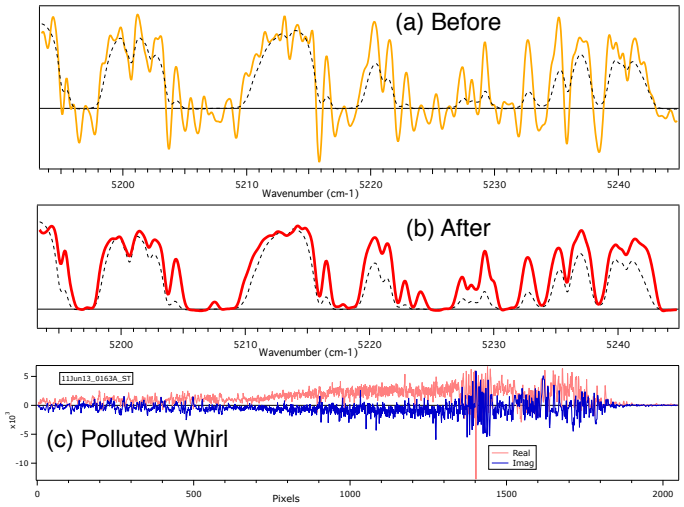

Fig. 4. A confirmation that the phase stepping algorithm is working properly is the lack of ringing artifact in the final spectra (red curve in panel b). Early processed spectra (yellow curve in panel a) had ringing in areas of spectrum that should be zero because of heavy telluric absorption, (dashed curve [8]). We traced the source of the problem to pollution (c) of the fringing spectrum (whirl) with a small amount of nonfringing, which creates a nearly zero frequency pedestal. This pedestal becomes a ringing artifact when the whole signal is Fourier shifted as part of the processing to produce a high resolution spectra. Changing a method of normalization solved the problem.

Since there are more phase steps than degrees of freedom, there are many possible weighting schemes. In our presentation we describe a generic but programmatically simple algorithm, along with methods of determining step delay, phase and visibility, and intensity normalization to use, iteratively, starting from unknown values.

1.2. Confirmation in Heavily Telluric Spectrum

Confirmation of success of the algorithm in separating the nonfringing component from fringing component is in Fig. 4[b], which shows the final high resolution output having no ringing artifact. Earlier algorithm versions which did not properly remove the nonfringing component manifested a ringing artifact, which was most easily apparent in the deeply absorptive telluric region of spectrum where the signal should be near zero.

This material is based upon work supported by the National Science Foundation under Grant No. AST-0505366, AST-096064, NASA Grant NNX09AB38G, and by Lawrence Livermore Nat. Lab. under Contract DE-AC52-07NA27344.

References

1. D. J. Erskine, "An externally dispersed interferometer prototype for sensitive radial velocimetry: theory and demonstration on sunlight," PASP **115**, 255–269 (2003).
2. D. J. Erskine, "Combined dispersive/interference spectroscopy for producing a vector spectrum," US Patent **6,351,307** (2002).
3. P. S. Muirhead, J. Edelstein, D. J. Erskine, J. T. Wright, M. W. Muterspaugh, K. R. Covey, E. H. Wishnow, K. Hamren, P. Andelson, D. Kimber, T. Mercer, S. P. Halverson, A. Vanderburg, D. Mondo, A. Czeszumska, and J. P. Lloyd, "Precise stellar radial velocities of an M dwarf with a Michelson interferometer and a medium-resolution near-infrared spectrograph," PASP **123**, 709–724 (2011).
4. D. J. Erskine, J. Edelstein, M. Feuerstein, and B. Welsh, "High resolution broadband spectroscopy using an externally dispersed interferometer," ApJ **592**, L103–L106 (2003).
5. D. J. Erskine and J. Edelstein, "Interferometric resolution boosting for spectrographs," in "Ground-based Instrumentation for Astronomy," , vol. 5492 of *Proc. SPIE*, A. Moorwood and M. Iye, eds. (2004), vol. 5492 of *Proc. SPIE*, pp. 190–199.
6. D. J. Erskine, J. Edelstein, M. Sirk, E. Wishnow, Y. Ishikawa, E. McDonald, and W. V. Shourt, "High Resolution Broad-Band Spectroscopy in the NIR Using the TripleSpec Externally Dispersed Interferometer at the Hale Telescope," in "Ground-based and Airborne Instrumentation V," , vol. 9147 of *Proc. SPIE* (2014), vol. 9147 of *Proc. SPIE*, p. 914717.
7. J. Greivenkamp and J. Bruning, "Phase Shifting Interferometry," in "Optical Shop Testing," , D. Malacara, ed. (John Wiley & Sons, 1992), chap. 14, pp. 501–598, 2nd ed.
8. H. G. Roe, "Titan's atmosphere at high-resolution," Ph.D. thesis, Univ. California, Berkeley (2002).